Integral Backstepping Sliding Mode Control for Maximizing the Power Production of Wind Turbines

Habiba Abouri
Systems Engineering and Information Technologies Laboratory, ENSA, Morocco
abourihabiba@gmail.com (corresponding author)

Fatima El Guezar
Systems Engineering and Information Technologies Laboratory, ENSA, Morocco
fatima.elguezar@uiz.ac.ma

Hassane Bouzahir
Systems Engineering and Information Technologies Laboratory, ENSA, Morocco
hbouzahir@yahoo.fr

Seif Eddine Chehaidia
Ecole Nationale Polytechnique de Constantine, Algeria
seifeddinechehaidia@yahoo.fr

Alessandro N. Vargas
Universidade Tecnologica Federal do Parana, Brazil
avargas@utfpr.edu.br

Received: 4 November 2023 | Revised: 30 November 2023 and 14 December 2023 | Accepted: 19 December 2023

 DOI: https://doi.org/10.48084/etasr.6592

ABSTRACT

Wind turbine control has attracted increasing attention, driven in part by evolving challenges due to the growing size and complexity of wind turbines. Addressing these challenges and maximizing wind turbine power production requires the application of advanced nonlinear control methods. Sliding Mode Control (SMC) has emerged as a promising approach in this context. Recent studies have explored the integration of an integral term with SMC, called I-SMC. This technique has been shown to result in system responses that exhibit chattering phenomena with noticeable state errors. This study aimed to address these issues through the introduction of a novel controller known as Integral Backstepping SMC (IB-SMC). This study demonstrated that IBSMC not only ensured the stability of wind turbines but also outperformed other control strategies, even in the presence of disturbances of approximately 30% of the rated electromagnetic torque. To validate the effectiveness of the proposed controller, extensive simulation tests were carried out using MATLAB /Simulink software to evaluate the controller's responsiveness to rapid changes in conditions, as well as its robustness and overall performance. A comparison was carried out between the IBSMC and previous SMCs to evaluate their ability to reduce steady-state error and chattering.

Keywords-wind turbines; stability; integral sliding mode control; backstepping control; nonlinear systems

I. INTRODUCTION

The last few years have seen an increase in interest in the control of wind turbines, partially motivated by the increasing complexity associated with the management of such large devices [1-4]. The bigger the turbines, the more challenges researchers face in designing their control. To complicate this scenario even further, researchers must consider which control works best when the wind turbine operates at variable or fixed rotor speed. When in operation, wind turbines can move between two distinct modes, called partial load and full load. For the partial-load case, the control objective is to maintain a steady tip-speed ratio and use this information to extract the maximum possible energy by tracking the wind and the turbine shaft speeds. However, in the full-load case, the control objective is to maintain the generator speed at its rated value

independently of the wind speed [1, 3, 5]. The control of wind turbines comprises two clear goals:

- Maximizing power production when the turbine operates at its normal speed
- Regulating power production at a specific level when the wind speed exceeds a certain threshold.

A wide range of control methods have been proposed to maximize power production, including linear, nonlinear, and data-driven control [1, 3, 6-8]. Although linear control methods have shown promising results [9], many studies have shown that nonlinear control for wind turbines outperforms linear control [2-3, 7]. Sliding Mode Control (SMC) has attracted attention and has been widely used to control nonlinear processes subjected to external disturbances [10-13]. A switching function, known as the sliding manifold, is selected to drive the system trajectories to reach the manifold (i.e. the sliding surface). This means that all system trajectories will reach the sliding surface and will remain there forever [11, 13].

In terms of wind turbines, SMC has proved its effectiveness in wind turbine control. In [5], promising results were achieved when using SMC based on the Utkin method and considering a two-mass drive train model with integral action to minimize errors. In [14], the Utkin method was applied in the setup of a single mass model with fuzzy representation. In [15], the importance of SMC for wind turbines was presented, showing improvements when SMC works with a time-varying compensator to compute the sliding surface. I-SMC has gained popularity because the integral term ensures that the system error goes to zero as the system evolves. As with SMC, I-SMC relies upon a sliding surface that drives the system state to a desired equilibrium point and the additional integral term helps to eliminate the steady-state error. I-SMC improves the performance of wind turbines in the presence of disturbances [16]. In [17], I-SMC was proposed when extracting maximum power at below-rated wind speed [17]. In [18], I-SMC was investigated to improve the performance of permanent magnet synchronous wind turbine generators [18]. Backstepping [19] is a nonlinear control strategy that, combined with SMC, can significantly improve the process response, for example, in photovoltaics [20], robot manipulators [21], vehicles [22], quadrotors [23], and wind turbines [24-25]. In [24-25], the benefits of backstepping with SMC were presented. However, tracking has not yet been fully solved under backstepping with SMC. Tracking requires an integral term, recall, to drive the system to the desired tracking point. In [24-25] backstepping was used with SMC (B-SMC) in the context of wind turbines, but B-SMC does not ensure tracking. However, IB-SMC ensures tracking. IB-SMC has already been investigated in other contexts, such as DFIG [6, 26], quadrotors [27] magnetic levitation [28], optoelectronic platforms [29], and photovoltaic energy [30]. This study contributes toward this direction by presenting a strategy that joins the integral term with both backstepping and SMC, contributing the following:

- IB-SMC is proposed for wind turbines to reduce chattering by giving a high nonlinearity on the switching manifold using inner loops.
- The chattering problem of SMC due to the linearity of the sliding surface is addressed.
- An integral term is considered to improve the precision of the system, as concluded from I-SMC.
- The robustness and closed-loop stability of the proposed control law is tested.
- The controller's parameters are ptimized to meet the required objectives in terms of stability, precision, and chattering mitigation.

II. MODELING

Wind turbines depend on certain mechanical and electric elements to produce electricity. The aerodynamic power extracted from the turbine's shaft is given by [3, 8, 31]:

$$P_a = \frac{1}{2}\rho\pi C_p(\lambda,\beta)v^3R^2 \quad (1)$$

where R, v, and ρ denote the rotor radius, wind speed, and air density (kg/m^3), respectively. C_p is the turbine's aerodynamic efficiency that is highly dependent on the tip speed ratio (λ) and the blade pitch angle (β). According to Betz's limit, the power factor $C_p(\lambda, \beta)$ never exceeds the value of 0.593 [32]. The tip-speed ratio λ is given by (2) [24, 33]:

$$\lambda = \frac{R\omega_r}{v} \quad (2)$$

where ω_r is the rotational speed of the wind turbine. The power coefficient $C_p(\lambda, \beta)$ required in (1) can be expressed by [34]:

$$C_p(\lambda,\beta) = 0.0068\lambda + 0.5176\left(\frac{116}{\eta} - 0.4\beta - 5\right)e^{(-21\eta^{-1})} \quad (3)$$

with η satisfying: $\frac{1}{\eta} = \frac{1}{(\lambda+0.08\beta)} - \frac{0.035}{(\beta^3+1)}$.

Aerodynamic torque is expressed as follows [17, 35-36]:

$$T_a = \frac{1}{2\lambda}\rho\pi R^3 C_p(\lambda,\beta)v^2 \quad (4)$$

A. Power Transmission Modeling

The mechanism of a wind turbine contains a drivetrain, which names the group of gears that make the conversion of mechanical energy from the low-speed shaft to the electric generator. The corresponding equations are [39]:

$$J_r\dot{\omega}_r = T_a - T_{ls} - K_r\omega_r \quad (5)$$

$$J_g\dot{\omega}_g = T_{hs} - K_g\omega_g - T_{em} \quad (6)$$

where T_a (T_{ls}) is the aerodynamic (low-speed) shaft torque. Low-speed shaft speed is denoted by ω_{ls}, and rotor side (generator side) angular deviation is denoted by ω_r (ω_g). The high-speed shaft torque T_{hs} propels the generator's inertia J_g while the generator torque T_g and the generator dampening K_g act as brakes. Since the low-speed and high-speed shaft torque are related through the rule T_{ls}=N_gT_{hs}, (6) can be used to write:

$$T_{ls} = N_g\left(J_g\dot{\omega}_g + K_g\omega_g + T_{em}\right) \quad (7)$$

Combining (5) and (7) gives:

$$J_r\dot{\omega}_r = T_a - T_{ls} - K_r\omega_r \quad (8)$$

III. CONTROL SYSTEM

Wind turbines are designed to generate electricity as efficiently as possible. Industrial wind turbines achieve maximum power efficiency when the wind crosses the turbine blades at a speed of 10 to 15 m/s [8]. When the wind speed exceeds 15 m/s, the turbine can be damaged and a safer strategy is to slow down the shaft speed. In this case, all additional power that could be extracted from the wind must be discharged. Industrial wind turbines have a built-in power-regulation mechanism for any kind of wind. When the output power is lower than the rated power, wind turbines must respond to rapid variations. Typically, the turbine operates at variable rotor speeds to capture the maximum available wind energy, and the torque generator provides input control by varying the rotor speed while keeping the blade pitch angle constant. Various control methods have been proposed, some combining linear and nonlinear control techniques or employing more advanced control strategies. Most of these methods involve multiple objectives and some of them aim to control the rotor speed reference.

This study aims to design a control method that maximizes power extraction. This was achieved under the following considerations. Controlling wind turbines usually requires dealing with two inputs and two outputs [14, 40]. In formal terms, the two inputs are the blade pitch angle β_{reg} and the electromagnetic torque of the generator T_{em}. The two outputs are the generated electrical power P and the turbine rotation speed ω_r. Both β and λ in (1) are maintained at their optimal values to achieve the control goal. In particular, to obtain the optimal value for λ, the rotor speed ω_r must follow the optimal reference rotor speed ω_{ropt}. This is achieved by modifying the control input signal T_g.

A. Baseline Control

Baseline control denotes the classical control strategy that regulates the generator torque to maximize power output at varying wind speeds. This control strategy is the most commonly used and studied controller in wind turbines [1-3]. The baseline control works as follows. The turbine sets the blade pitch angle to zero to extract the maximum energy. Afterward, the wind turbine operates under generator torque control T_g through [5, 41]:

$$T_g = \frac{1}{2\lambda_{opt}^3}\rho\pi R^5 C_{pmax}\omega_r^2 \quad (9)$$

B. Sliding Mode Control

Although SMC has been successfully applied in the control of wind turbines, it is known to have a side effect: SMC creates chattering, a phenomenon that makes the system oscillate with increasing frequency [12]. Several attempts have been made to mitigate the impact of chattering. One of them is to apply control with saturation or hyperbolic tangent functions. The control law then ensures that the system remains on the sliding surface, and any abrupt changes in the control are replaced by a smoother variation function, which is then added to the continuous control term. This feature is recalled in the sequence.

There are two significant steps in the SMC design process. The first is to define the switching surface to achieve the required system dynamics. To extract the maximum power at below-rated wind speed (e.g. 15 m/s), the turbine rotor speed must track the reference rotor speed, which is derived from the effective wind speed. The second step is to choose the control law that drives the trajectories to the switching surface. For both steps, the sliding surface can be defined by [24, 35, 42]. The corresponding asymptotic stability is ensured if the Lyapunov function $V = S^2$ satisfies $\dot{V} = S, \dot{S} < 0$, following:

$$\dot{V} = S\left(\frac{T_a}{J_r} - \frac{K_r}{J_r}\omega_r - \frac{N_g J_g}{J_r}\dot{\omega}_g - \frac{N_g K_g}{J_r}\omega_g - \frac{N_g}{J_r}T_{em} - \dot{\omega}_{ref}\right) \quad (10)$$

where T_{em} represents the control law applied in the wind turbine. The scalar terms u_{equ} and u_{disc} are defined as:

$$u_{equ} = \frac{T_a}{N_g} - \frac{K_r}{N_g}\omega_r \pm \dot{\omega}_g - K_g\omega_g - \frac{J_r}{N_g}\dot{\omega}_{ref}$$

$$u_{disc} = -K\tanh\left(\frac{S}{\phi}\right), K > 0 \quad (11)$$

where K represents a proportional gain and $\varphi > 0$ is a constant related to the region around the desired operating point. The control law applied in the wind turbine is:

$$T_{em} = u = u_{equ} + u_{disc} = \frac{T_a}{N_g} - \frac{K_r}{N_g}\omega_r$$

$$-J_g\dot{\omega}_g - K_g\omega_g - \frac{J_r}{N_g}\dot{\omega}_{ref} - Ktanh\left(\frac{S}{\phi}\right) \quad (12)$$

C. Integral Sliding Mode Control

Conventional SMC acts to minimize the error between the measured output and the desired operating point [34]. However, this strategy sometimes leads to a slow convergence to the desired operating point, especially if the system has a steady-state error. I-SMC incorporates an integral term to minimize the tracking error [2, 35]. Formally, the I-SMC reads as [31, 43-44]:

$$S(t) = e(t) + K_i\int_0^\infty e(t)dt \quad (13)$$

with $e(t) = \omega_r(t) - \omega_{ref}(t)$. Considering the Lyapunov function as $V = S^2$, gives:

$$\dot{V} = S\left(\dot{e}(t) + K_i e(t)\right) = S(\frac{T_a}{J_r} - \frac{K_r}{J_r}\omega_r - \frac{N_g J_g}{J_r}\dot{\omega}_g$$

$$-\frac{N_g K_g}{J_r}\omega_g - \frac{N_g}{J_r}T_{em} - \dot{\omega}_{ref} + K_i e(t)) \quad (14)$$

Then, obtain $\dot{V} < 0$ whenever the control torque T_{em} satisfies:

$$T_{em} = \frac{T_a}{N_g} - \frac{K_r}{N_g}\omega_r - J_g\dot{\omega}_g - K_g\omega_g - \frac{J_r}{N_g}\dot{\omega}_{ref}$$

$$+\frac{J_r}{N_g}K_i e(t) - K\tanh\left(\frac{S}{\phi}\right) \quad (15)$$

D. Integral-Backstepping SMC (IB-SMC)

IB-SMC combines I-SMC with backstepping [45-47]. Like the I-SMC, IB-SMC handles and minimizes the error as quickly as possible. Backstepping transforms lower-order systems into a strict feedback form [24, 43, 48]. The integral-backstepping technique can be adapted and merged with SMC to generate a smooth output signal, thereby removing any

chattering in the control input. IB-SMC is an important step in overcoming certain limitations of conventional SMC, such as chattering, steady-state error, and tracking errors resulting from uncertainties and disturbances. Compared to traditional backstepping control, the integration of integral backstepping with SMC improves robustness against external disturbances by avoiding discontinuous control signals and improving tracking accuracy.

The tracking error ε_1 is defined as :

$$\varepsilon_1 = \omega_r - \omega_{ref} \quad (16)$$

As usual, the goal is to ensure that ε_1 tends to zero as t tends to infinity. Taking the derivative to time on both sides of (16), with (8) gives:

$$\dot{\varepsilon}_1 = \frac{T_a}{J_r} - \frac{K_r}{J_r}\omega_r - \frac{N_g J_g}{J_r}\dot{\omega}_g - \frac{N_g K_g}{J_r}\omega_g - \frac{N_g}{J_r}T_{em} - \dot{\omega}_{ref} \quad (17)$$

The candidate Lyapunov function is:

$$V_1 = \frac{1}{2}\varepsilon_1^2 + k\frac{1}{2}\xi^2 \quad (18)$$

where $\xi(t) = \int_0^t (\omega_r - \omega_{ref})dt$ is the rotor speed error. The first time derivative of (18), is:

$$\dot{V}_1 = \varepsilon_1\left(\frac{T_a}{J_r} - \frac{K_r}{J_r}\omega_r - \frac{N_g J_g}{J_r}\dot{\omega}_g - \frac{N_g K_g}{J_r}\omega_g - \frac{N_g}{J_r}T_{em} - \dot{\omega}_{ref} + k\xi\right) \quad (19)$$

$K_1 > 0$ is defined as the constant that satisfies $\dot{V}_1 = -K_1\varepsilon_1^2$, resulting in:

$$-K_1\varepsilon_1 = \frac{T_a}{J_r} - \frac{K_r}{J_r}\omega_r - \frac{N_g J_g}{J_r}\dot{\omega}_g - \frac{N_g K_g}{J_r}\omega_g - \frac{N_g}{J_r}T_{em} - \dot{\omega}_{ref} + k\xi \quad (20)$$

The T_{em} variable is considered a virtual control input, meaning that it will drive (17) to the equilibrium zero point. A stabilizing function ς is derived, which is assumed to be identical to the virtual control input T_{em} to lead to the desired stability. The stabilizing function is defined as:

$$\varsigma = \frac{T_a}{N_g} - \frac{K_r}{N_g}\omega_r - J_g\dot{\omega}_g - K_g\omega_g - \frac{J_r}{N_g}\dot{\omega}_{ref} + \frac{J_r}{N_g}K\xi \quad (21)$$

The second error variable is defined as:

$$\varepsilon_2 = T_{em} - \varsigma \quad (22)$$

Substituting (22) into (17) gives:

$$\dot{\varepsilon}_1 = \frac{T_a}{J_r} - \frac{K_r}{J_r}\omega_r - \frac{N_g J_g}{J_r}\dot{\omega}_g - \frac{N_g K_g}{J_r}\omega_g - \dot{\omega}_{ref} - \frac{N_g}{J_r}(\varsigma) \quad (23)$$

Combining (18) and (20) gives:

$$\dot{\varepsilon}_1 = -K_1\varepsilon_1 - K\xi - \frac{N_g}{J_r}\varepsilon_2 \quad (24)$$

As a result, using (15) gives:

$$\dot{V}_1 = \varepsilon_1\dot{\varepsilon}_1 + K\xi\dot{\xi} = -K_1\varepsilon_1^2 - \frac{N_g\varepsilon_1\varepsilon_2}{J_r} \quad (25)$$

It should be noted that the term $-K_1\varepsilon_1^2$ is negative. However, the term $N_g\varepsilon_1\varepsilon_2/J_r$ can become either positive or negative when $t > 0$ increases. The next argument is introduced to ensure that $N_g\varepsilon_1\varepsilon_2/J_r$ becomes negative for all $t > 0$, and so ensuring that $\dot{V}_1$ is negative for all $t > 0$, following (21) and (22):

$$\dot{\varsigma} = \frac{\dot{T}_a}{N_g} - \frac{K_r}{N_g}\dot{\omega}_r - J_g\ddot{\omega}_g - K_g\dot{\omega}_g - \frac{J_r}{N_g}\ddot{\omega}_{ref} + \frac{J_r}{N_g}K\dot{\xi} + \frac{J_r}{N_g}K_1\dot{\varepsilon}_1 \quad (26)$$

Hence:

$$\dot{\varepsilon}_2 = \dot{T}_{em} - \frac{\dot{T}_a}{N_g} + \frac{K_r}{N_g}\dot{\omega}_r + J_g\ddot{\omega}_g + K_g\dot{\omega}_g + \frac{J_r}{N_g}\ddot{\omega}_{ref} - \frac{J_r}{N_g}K\dot{\xi} - \frac{J_r}{N_g}K_1\dot{\varepsilon}_1 \quad (27)$$

According to Step 2, the Lyapunov function becomes [30]:

$$V_2 = V_1 + \frac{1}{2}\varepsilon_2^2 \quad (28)$$

which implies:

$$\dot{V}_2 = \dot{V}_1 + \varepsilon_2\dot{\varepsilon}_2 = -K_1\varepsilon_1^2 - \frac{N_g\varepsilon_1\varepsilon_2}{J_r} + \varepsilon_2\dot{\varepsilon}_2 = -K_1\,\varepsilon_1^2 + \varepsilon_2\left(\dot{\varepsilon}_2 - \frac{N_g\varepsilon_1}{J_r}\right) \quad (29)$$

To ensure the stability of $\dot{V}_2$, let us set:

$$\dot{\varepsilon}_2 - \frac{N_g\varepsilon_1}{J_r} = -K_2\varepsilon_2 \quad (30)$$

Under this condition set, the following is achieved:

$$\dot{V}_2 = -K_1\varepsilon_1^2 - K_2\varepsilon_2^2 < 0 \quad (31)$$

which implies the asymptotic stability to the zero point. To conclude the reasoning, (28) and (30) are combined to obtain:

$$\dot{T}_{em} = \frac{\dot{T}_a}{N_g} - \frac{K_r}{N_g}\dot{\omega}_r - J_g\ddot{\omega}_g - K_g\dot{\omega}_g - \frac{J_r}{N_g}\ddot{\omega}_{ref} + \frac{J_r}{N_g}K\dot{\xi} + \frac{J_r}{N_g}K_1\dot{\varepsilon}_1 + \frac{N_g\varepsilon_1}{J_r} - K_2\varepsilon_2 \quad (32)$$

The control term T_{em} is obtained by integrating the last expression:

$$T_{em} = \frac{T_a}{N_g} - \frac{K_r}{N_g}\omega_r - J_g\dot{\omega}_g - K_g\omega_g - \frac{J_r}{N_g}\dot{\omega}_{ref} + \frac{J_r}{N_g}K\xi + \frac{J_r}{N_g}K_1\varepsilon_1 + \frac{N_g\xi}{J_r} - K_2\int_0^t \varepsilon_2(\tau)d\tau \quad (33)$$

IB-SMC consists of two components, i.e.:

$$u_{IB-SMC} = T_{em} + u_{disc} \quad (34)$$

where T_{em} satisfies (32) and u_{disc} satisfies:

$$u_{disc} = -K\tanh\left(\frac{S}{\phi}\right) \quad (35)$$

SMC brings the benefit of fast-tracking for the desired trajectory. On the other hand, backstepping control brings the benefit of avoiding chattering and adding the integral term that ensures the system reaches zero steady-state error. As summarized in (33), IB-SMC brings into a unique setup the benefits of both SMC and integral backstepping control.

IV. RESULTS AND DISCUSSION

The simulation of the proposed controller was divided into two parts: the first involves typical trajectory tracking without disturbances, while the second focuses on rotor speed tracking under external disturbances. Various control methods, including conventional control [49-50], SMC [51], I-SMC, and IB-SMC, were simulated to compare their tracking accuracy and robustness against external disturbances. IB-SMC was evaluated by simulating a two-mass wind turbine model in MATLAB/Simulink. It was a 600 kW CART3 variable-speed wind turbine model [15], and Table I details its variable-pitch characteristics.

A. Output Power Analysis

IB-SMC was compared with baseline, SMC, and I-SMC. The IB-SMC parameters were K = 0.1, K_1 = 0.3, and K_2 = 0.0001. The other methods were simulated with K = 0.145 and K_i = 0.001. The wind speed was kept the same in all experiments, according to the procedure described in [24], with a mean value of 8 m/s. Figure 1 shows the power produced by the wind turbine model using different control strategies. All control methods guided the model to its maximum power production, which varied greatly during short periods. To fairly grasp this information, the total amount of power produced was calculated for each control strategy. Table II summarizes the corresponding data, showing that IB-SMC outperformed all competitors, increasing efficiency by approximately 0.26% and proving the potential benefits of IB-SMC for wind turbines.

TABLE I. DATA FOR WIND TURBINE SIMULATIONS. VALUES USED IN THE SIMULATIONS

Symbol	Notation	Value	Units
R	Turbine rotor radius	21.65	M
ρ	Air density	1.225	kg/m^3
J_r	Rotoris inertial mass	3.25×10^5	kg.m^2
K_{ls}	Shaft damping	9500	N.m/rad/s
B_{ls}	Shaft stiffness	2.691×10^5	N.m/rad
K_r	Rotor's friction	27.36	N.m/rad/s
K_g	Generator friction	0.2	N.m/rad/s
J_g	Generator inertial mass	34.4	kg.m^2
T_a	Maximum electrical torque	3.753×10^5	N.m
N_g	Gearbox ratio	41.165	-
λ	Optimal tip ratio speed	8.5	-

TABLE II. POWER PRODUCTION UNDER DISTINCT CONTROL STRATEGIES

Criterion	Baseline	SMC	I-SMC	IB-SMC
P_{max} (kW)	218.33	218.31	218.27	218.91

B. Vibration Mitigation Analysis

Wind turbines are subjected to a wide range of vibrations, both from external and internal sources. The most significant external vibrations are caused by wind gusts and turbulence, which can cause the blades and the tower to shake and vibrate [53]. Internal vibrations can be caused by imbalances in the rotating components or other issues related to the support structures. In any case, excessive vibration can lead to fatigue and permanent damage to turbine components. In some circumstances, control can mitigate or amplify vibrations, as confirmed by simulations. Figure 2 shows that the IB-SMC decreased the vibrations in the turbine model, in contrast to the other strategies that generated higher vibrations. This finding suggests that using IB-SMC to control wind turbines has the potential to protect the turbine mechanisms against vibrations.

C. Performance Comparison

The main control objective was to maximize power capture from the wind turbine by accurately tracking the rotor speed. Figure 3 shows the rotor speed for the following controllers: baseline, SMC, I-SMC, and IB-SMC. IB-SMC seems to track the optimal rotor speed, which is confirmed by the computed error shown in Table III. Figures 4 and 5 show the low-speed shaft torque and the electromagnetic torque response. IB-SMC showed lower oscillations when compared to SMC and I-SMC, however, the baseline seems to produce the lowest oscillations.

TABLE III. TRACKING ERROR OF THE ROTOR SPEED UNDER DISTINCT CONTROL STRATEGIES

Criterion	Baseline	SMC	I-SMC	IB-SMC
Error (%)	2.6	3.1	2.3	1

Table IV shows a comparison between the proposed and the conventional controllers. The following terms were used to compare the efficiency of the controllers: electrical efficiency (η_{elec}) and aerodynamic efficiency (η_{aero}). Aerodynamic efficiency is the ratio of energy captured by the wind turbine to the optimal energy available from the wind and can be mathematically expressed as:

$$\eta_{aero}(\%) = \frac{\int_{t_{ini}}^{t_{fin}} P_a(t)\,dt}{\int_{t_{ini}}^{t_{fin}} P_{aopt}(t)\,dt} \quad (36)$$

Electrical efficiency is the ratio of electric energy produced to the optimal energy available from the wind, and is given by:

$$\eta_{elec}(\%) = \frac{\int_{t_{ini}}^{t_{fin}} P_e(t)dt}{\int_{t_{ini}}^{t_{fin}} P_{aopt}(t)dt} \quad (37)$$

The optimal aerodynamic torque is given by:

$$P_{aopt} = \frac{1}{2}\rho\pi R^2 C_{Pmax} v^3 \quad (38)$$

TABLE IV. COMPARISON OF DIFFERENT CONTROL STRATEGIES USING η_{elec} AND η_{aero}

Indicator	Baseline	SMC	I-SMC	IB-SMC
η_{ele}(%)	97.0	98.6	97.7	98.5
η_{aero}(%)	70.28	70.35	70.12	70.40
Max T_{em} (kNm)	1.625	1.626	1.627	1.642
Std T_{em} (kNm)	0.643	0.460	0.372	0.210

Figure 6 shows a variable wind profile with rapid peak changes [53], which was used to examine the effectiveness of the proposed controller. Figure 7 shows the rotor speed with a disturbance level of 5 kNm. The SMC and ISMC could not follow the reference rotor speed, resulting in a considerably reduced efficiency. In proportional control, the rotor speed deviates from the reference value and is influenced by all disturbance levels, while any adjustments on the pitch angle result in lower power than the intended rotor speed's extracted power value. The IB-SMC can adapt to the 10 kNm

disturbance level while maintaining the tracking of the desired rotor speed value. The main objective of the controllers is to maximize energy capture while reducing transmission stresses. The results show that the power captured from the reference rotor value remains almost unchanged for the IBSMC, even with a twofold increase in disturbance levels from 5 to 10 kNm. Unlike SMC and ISMC, power efficiency was affected by the 5 kNm disturbance, and proportional control was also influenced by disturbance and changes in pitch angle. Table V compares the performance and complexity of the controllers, showing that the baseline and SMC controllers have low complexity and performance. The I-SMC controller has low complexity and moderate performance, which is consistent with [35]. The results indicate that the IB-SMC is the most complex and also the most effective controller among the four.

TABLE I. COMPARISON OF ELECTROMAGNETIC TORQUE CONTROLLERS

Controller	Complexity	Performance
Baseline	Low	Low
SMC	Low	Low
I-SMC	Low	Moderate
IB-SMC	High	High

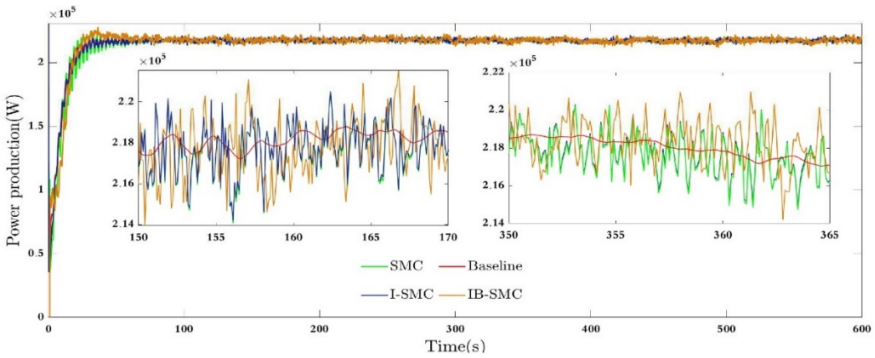

Fig. 1. Wind turbine simulation: power produced by distinct control strategies.

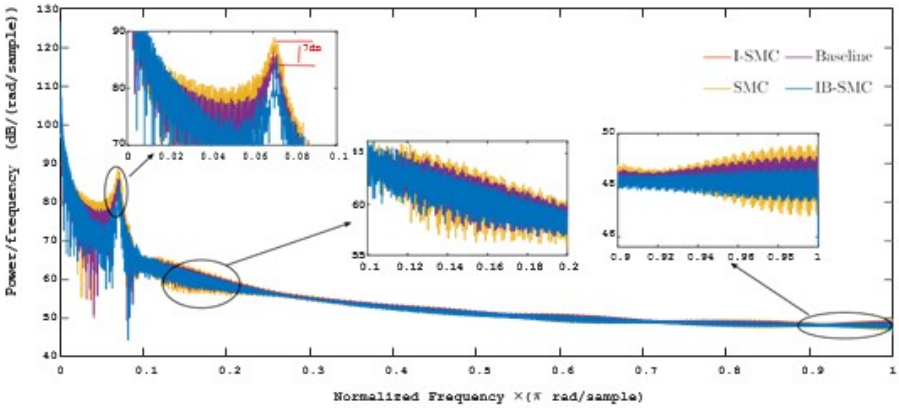

Fig. 2. Power spectral density of T_{ls}: the greater the amplitude, the greater the vibration. IB-SMC seems to generate the lowest amplitudefor most frequencies.

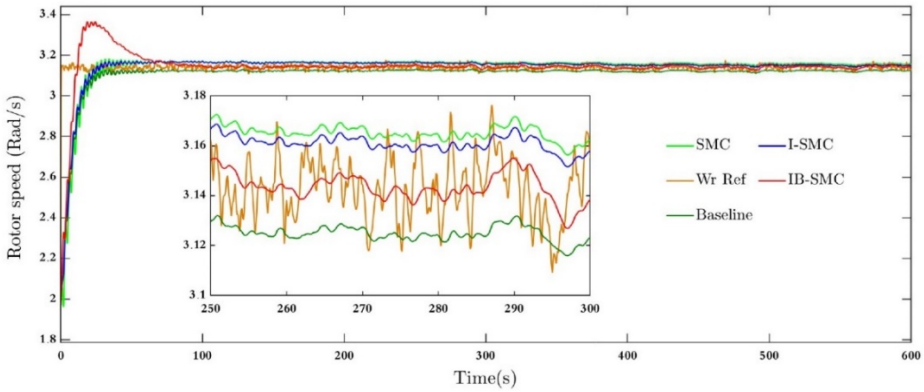

Fig. 3. Rotor speed comparison for SMC, I-SMC, and IB-SMC.

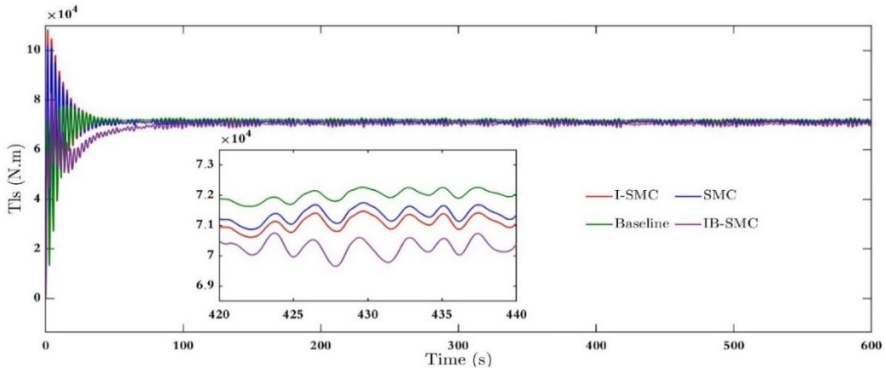

Fig. 4. Low-speed shaft torque comparison for SMC, I-SMC, and IB-SMC.

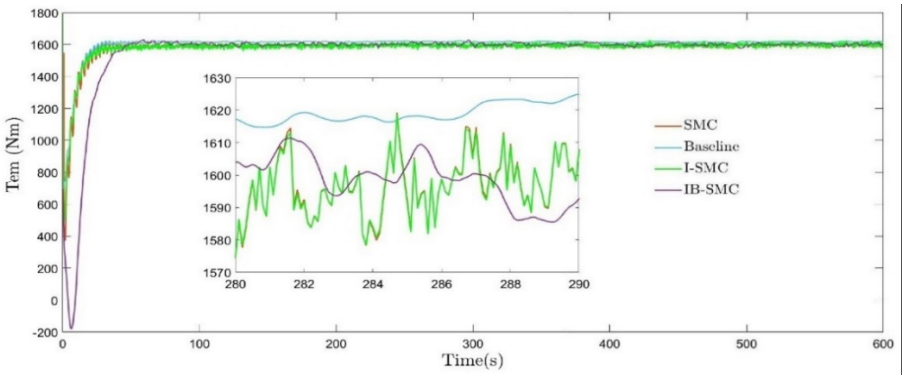

Fig. 5. Electromagnetic torque comparison for SMC, I-SMC, and IB-SMC.

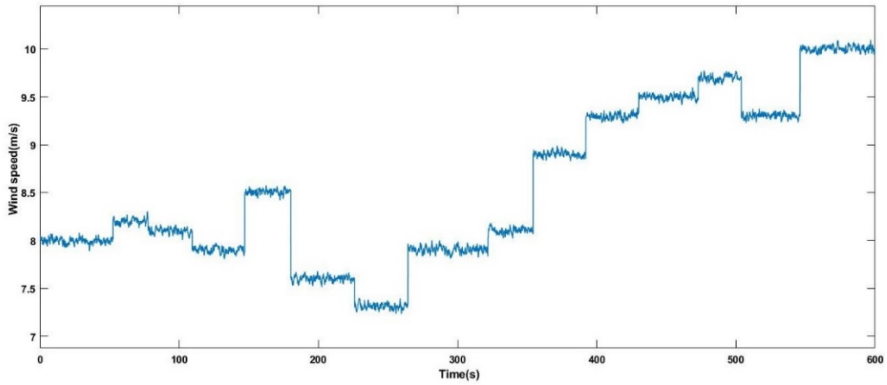

Fig. 6. Wind speed profile.

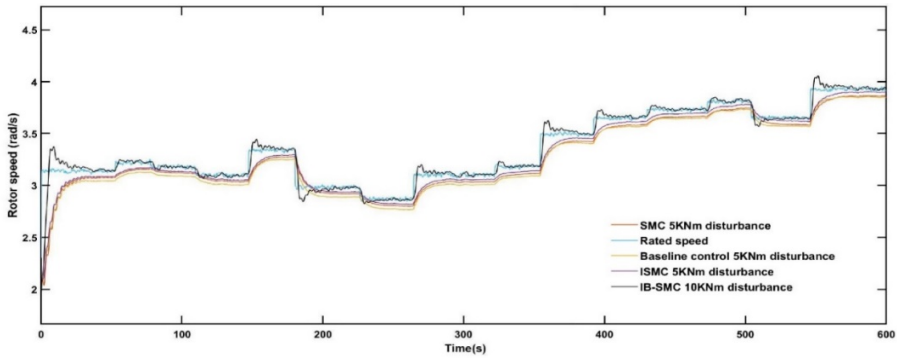

Fig. 7. Rotor speed comparison for SMC, I-SMC, and IB-SMC with 5 kNm disturbance.

V. CONCLUSION

This paper introduced a novel control strategy for wind turbines termed as IB-SMC. This strategy combines the advantages of I-SMC, which facilitates tracking of the desired trajectory with backstepping control, which is known to prevent chattering and compensate for the steady-state error. In addition, IB-SMC ensures the stability of wind turbines. Comparative analysis was performed against the baseline, conventional SMC, and I-SMC, and simulation results showed that IB-SMC surpassed them in terms of power production, exhibiting an approximately 0.26% increase in efficiency. IB-SMC also demonstrated the ability to generate the lowest vibration amplitude in the turbine model, indicating its potential application to protect turbine mechanisms against vibrations. In conclusion, the simulations and result comparison underscored the potential advantages of the proposed IB-SMC strategy for wind turbines.

REFERENCES

[1] L. Y. Pao and K. E. Johnson, "Control of Wind Turbines," *IEEE Control Systems Magazine*, vol. 31, no. 2, pp. 44–62, Apr. 2011, https://doi.org/10.1109/MCS.2010.939962.

[2] E. J. Novaes Menezes, A. M. Araújo, and N. S. Bouchonneau da Silva, "A review on wind turbine control and its associated methods," *Journal of Cleaner Production*, vol. 174, pp. 945–953, Feb. 2018, https://doi.org/10.1016/j.jclepro.2017.10.297.

[3] J. G. Njiri and D. Söffker, "State-of-the-art in wind turbine control: Trends and challenges," *Renewable and Sustainable Energy Reviews*, vol. 60, pp. 377–393, Jul. 2016, https://doi.org/10.1016/j.rser.2016.01.110.

[4] C. Anderson, *Wind Turbines: Theory and Practice*. Cambridge University Press, 2020.

[5] S. Rajendran and D. Jena, "Control of Variable Speed Variable Pitch Wind Turbine at Above and Below Rated Wind Speed," *Journal of Wind Energy*, vol. 2014, Oct. 2014, Art. no. e709128, https://doi.org/10.1155/2014/709128.

[6] H. Chojaa *et al.*, "Advanced Control Techniques for Doubly-Fed Induction Generators Based Wind Energy Conversion Systems," in *2022 Global Energy Conference (GEC)*, Batman, Turkey, Jul. 2022, pp. 282–287, https://doi.org/10.1109/GEC55014.2022.9987088.

[7] A. N. Vargas and L. Acho, "Optimal control of variable-speed wind turbines modeled as Markov jump systems," *Journal of the Franklin Institute*, vol. 359, no. 10, pp. 4661–4677, Jul. 2022, https://doi.org/10.1016/j.jfranklin.2022.05.006.

[8] S. Heier, *Grid Integration of Wind Energy: Onshore and Offshore Conversion Systems*. Hoboken, NJ, USA: John Wiley & Sons, 2014.

[9] B. Boukhezzar and H. Siguerdidjane, "Nonlinear Control of a Variable-Speed Wind Turbine Using a Two-Mass Model," *IEEE Transactions on Energy Conversion*, vol. 26, no. 1, pp. 149–162, Mar. 2011, https://doi.org/10.1109/TEC.2010.2090155.

[10] K. D. Young, V. I. Utkin, and U. Ozguner, "A control engineer's guide to sliding mode control," *IEEE Transactions on Control Systems Technology*, vol. 7, no. 3, pp. 328–342, Feb. 1999, https://doi.org/10.1109/87.761053.

[11] Y. Shtessel, C. Edwards, L. Fridman, and A. Levant, *Sliding Mode Control and Observation*. New York, NY, USA: Springer, 2014.

[12] V. Utkin, "Discussion Aspects of High-Order Sliding Mode Control," *IEEE Transactions on Automatic Control*, vol. 61, no. 3, pp. 829–833, Mar. 2016, https://doi.org/10.1109/TAC.2015.2450571.

[13] Y. Orlov, S. Chakrabarty, D. Zhao, and S. K. Spurgeon, "Sliding Mode Observer Design for a Parabolic PDE in the Presence of Unknown Inputs," *Asian Journal of Control*, vol. 21, no. 1, pp. 224–235, 2019, https://doi.org/10.1002/asjc.1849.

[14] S. Rajendran and D. Jena, "Variable speed wind turbine for maximum power capture using adaptive fuzzy integral sliding mode control," *Journal of Modern Power Systems and Clean Energy*, vol. 2, no. 2, pp. 114–125, Jun. 2014, https://doi.org/10.1007/s40565-014-0061-3.

[15] Y. Berrada and I. Boumhidi, "Sliding mode control for a wind turbine in finite frequency," *International Journal of Engineering Systems Modelling and Simulation*, vol. 10, no. 1, pp. 39–48, Jan. 2018, https://doi.org/10.1504/IJESMS.2018.090240.

[16] M. J. Morshed and A. Fekih, "Design of a chattering-free integral terminal sliding mode approach for DFIG-based wind energy systems," *Optimal Control Applications and Methods*, vol. 41, no. 5, pp. 1718–1734, 2020, https://doi.org/10.1002/oca.2635.

[17] R. Saravanakumar and D. Jena, "Validation of an integral sliding mode control for optimal control of a three blade variable speed variable pitch wind turbine," *International Journal of Electrical Power & Energy Systems*, vol. 69, pp. 421–429, Jul. 2015, https://doi.org/10.1016/j.ijepes.2015.01.031.

[18] C. Chatri, M. Ouassaid, M. Labbadi, and Y. Errami, "Integral-type terminal sliding mode control approach for wind energy conversion system with uncertainties," *Computers and Electrical Engineering*, vol. 99, Apr. 2022, Art. no. 107775, https://doi.org/10.1016/j.compeleceng.2022.107775.

[19] M. Krstic, I. Kanellakopoulos, and P. V. Kokotovic, *Nonlinear and Adaptive Control Design*, 1st edition. New York, NY, USA: Wiley-Interscience, 1995.

[20] K. Dahech, M. Allouche, T. Damak, and F. Tadeo, "Backstepping sliding mode control for maximum power point tracking of a photovoltaic system," *Electric Power Systems Research*, vol. 143, pp. 182–188, Feb. 2017, https://doi.org/10.1016/j.epsr.2016.10.043.

[21] D. T. Tran, D. X. Ba, and K. K. Ahn, "Adaptive Backstepping Sliding Mode Control for Equilibrium Position Tracking of an Electrohydraulic Elastic Manipulator," *IEEE Transactions on Industrial Electronics*, vol. 67, no. 5, pp. 3860–3869, Feb. 2020, https://doi.org/10.1109/TIE.2019.2918475.

[22] L. Zhang *et al.*, "An Adaptive Backstepping Sliding Mode Controller to Improve Vehicle Maneuverability and Stability via Torque Vectoring Control," *IEEE Transactions on Vehicular Technology*, vol. 69, no. 3, pp. 2598–2612, Mar. 2020, https://doi.org/10.1109/TVT.2019.2950219.

[23] X. Shi, Y. Cheng, C. Yin, S. Dadras, and X. Huang, "Design of Fractional-Order Backstepping Sliding Mode Control for Quadrotor UAV," *Asian Journal of Control*, vol. 21, no. 1, pp. 156–171, 2019, https://doi.org/10.1002/asjc.1946.

[24] S. Rajendran and D. Jena, "Backstepping sliding mode control of a variable speed wind turbine for power optimization," *Journal of Modern Power Systems and Clean Energy*, vol. 3, no. 3, pp. 402–410, 2015, https://doi.org/10.1007/s40565-015-0106-2.

[25] F. Echiheb *et al.*, "Robust sliding-Backstepping mode control of a wind system based on the DFIG generator," *Scientific Reports*, vol. 12, no. 1, Jul. 2022, Art. no. 11782, https://doi.org/10.1038/s41598-022-15960-7.

[26] H. Chojaa *et al.*, "Comparative Study of MPPT Controllers for a Wind Energy Conversion System," in *Advanced Technologies for Humanity*, 2022, pp. 300–310, https://doi.org/10.1007/978-3-030-94188-8_28.

[27] Z. Jia, J. Yu, Y. Mei, Y. Chen, Y. Shen, and X. Ai, "Integral backstepping sliding mode control for quadrotor helicopter under external uncertain disturbances," *Aerospace Science and Technology*, vol. 68, pp. 299–307, Sep. 2017, https://doi.org/10.1016/j.ast.2017.05.022.

[28] H. M. M. Adil, S. Ahmed, and I. Ahmad, "Control of MagLev System Using Supertwisting and Integral Backstepping Sliding Mode Algorithm," *IEEE Access*, vol. 8, pp. 51352–51362, 2020, https://doi.org/10.1109/ACCESS.2020.2980687.

[29] F. Yue, X. Li, C. Chen, and W. Tan, "Adaptive integral backstepping sliding mode control for opto-electronic tracking system based on modified LuGre friction model," *International Journal of Systems Science*, vol. 48, no. 16, pp. 3374–3381, Dec. 2017, https://doi.org/10.1080/00207721.2017.1387315.

[30] B. K. Oubbati, M. Boutoubat, A. Rabhi, and M. Belkheiri, "Experiential Integral Backstepping Sliding Mode Controller to achieve the Maximum

Power Point of a PV system," *Control Engineering Practice*, vol. 102, Sep. 2020, Art. no. 104570, https://doi.org/10.1016/j.conengprac.2020.104570.

[31] K. Palanimuthu, G. Mayilsamy, A. A. Basheer, S. R. Lee, D. Song, and Y. H. Joo, "A Review of Recent Aerodynamic Power Extraction Challenges in Coordinated Pitch, Yaw, and Torque Control of Large-Scale Wind Turbine Systems," *Energies*, vol. 15, no. 21, Jan. 2022, Art. no. 8161, https://doi.org/10.3390/en15218161.

[32] J. F. Manwell, J. G. McGowan, and A. L. Rogers, *Wind Energy Explained: Theory, Design and Application*. Hoboken, NJ, USA: John Wiley & Sons, 2010.

[33] S. E. Chehaidia, A. Abderezzak, H. Kherfane, B. Boukhezzar, and H. Cherif, "An Improved Machine Learning Techniques Fusion Algorithm for Controls Advanced Research Turbine (CART) Power Coefficient Estimation," *UPB Scientific Bulletin*, vol. 82, pp. 279–292, 2020.

[34] L. Pan, Z. Zhu, Y. Xiong, and J. Shao, "Integral Sliding Mode Control for Maximum Power Point Tracking in DFIG Based Floating Offshore Wind Turbine and Power to Gas," *Processes*, vol. 9, no. 6, Jun. 2021, Art. no. 1016, https://doi.org/10.3390/pr9061016.

[35] S. E. Chehaidia *et al.*, "Robust Nonlinear Terminal Integral Sliding Mode Torque Control for Wind Turbines Considering Uncertainties," *IFAC-PapersOnLine*, vol. 55, no. 12, pp. 228–233, Jan. 2022, https://doi.org/10.1016/j.ifacol.2022.07.316.

[36] S. E. Chehaidia *et al.*, "An Improved Supervised Fuzzy PI Collective Pitch Angle Control for Wind Turbine Load Mitigation," in *Digital Technologies and Applications*, Fez, Morocco, 2022, pp. 685–695, https://doi.org/10.1007/978-3-031-02447-4_71.

[37] E. Chavero-Navarrete, M. Trejo-Perea, J. C. Jáuregui-Correa, R. V. Carrillo-Serrano, and J. G. Ríos-Moreno, "Expert Control Systems for Maximum Power Point Tracking in a Wind Turbine with PMSG: State of the Art," *Applied Sciences*, vol. 9, no. 12, Jan. 2019, Art. no. 2469, https://doi.org/10.3390/app9122469.

[38] H. Abouri, F. E. Guezar, and H. Bouzahir, "Advanced Control Strategies for Wind Energy Systems," in *2020 International Conference on Electrical and Information Technologies (ICEIT)*, Rabat, Morocco, Mar. 2020, https://doi.org/10.1109/ICEIT48248.2020.9113193.

[39] A. Bektache and B. Boukhezzar, "Nonlinear predictive control of a DFIG-based wind turbine for power capture optimization," *International Journal of Electrical Power & Energy Systems*, vol. 101, pp. 92–102, Oct. 2018, https://doi.org/10.1016/j.ijepes.2018.03.012.

[40] A. R. periyanayagam and Y. H. Joo, "Integral sliding mode control for increasing maximum power extraction efficiency of variable-speed wind energy system," *International Journal of Electrical Power & Energy Systems*, vol. 139, Jul. 2022, Art. no. 107958, https://doi.org/10.1016/j.ijepes.2022.107958.

[41] M. Hannachi, O. Elbeji, M. Benhamed, and L. Sbita, "Optimal torque maximum power point technique for wind turbine: Proportional–integral controller tuning based on particle swarm optimization," *Wind Engineering*, vol. 45, no. 2, pp. 337–350, Apr. 2021, https://doi.org/10.1177/0309524X19892903.

[42] B. Yang, T. Yu, H. Shu, J. Dong, and L. Jiang, "Robust sliding-mode control of wind energy conversion systems for optimal power extraction via nonlinear perturbation observers," *Applied Energy*, vol. 210, pp. 711–723, Jan. 2018, https://doi.org/10.1016/j.apenergy.2017.08.027.

[43] S. Sumbekov, B. D. H. Phuc, and T. D. Do, "Takagi–Sugeno fuzzy-based integral sliding mode control for wind energy conversion systems with disturbance observer," *Electrical Engineering*, vol. 102, no. 3, pp. 1141–1151, Sep. 2020, https://doi.org/10.1007/s00202-020-00939-2.

[44] S. Zhang, S. Li, and F. Dai, "Integral Sliding Mode Backstepping Control of an Asymmetric Electro-Hydrostatic Actuator Based on Extended State Observer," *Proceedings*, vol. 64, no. 1, 2020, Art. no. 13, https://doi.org/10.3390/IeCAT2020-08495.

[45] L. Wang, L. Cao, and L. Zhao, "Non-linear tip speed ratio cascade control for variable speed high power wind turbines: a backstepping approach," *IET Renewable Power Generation*, vol. 12, no. 8, pp. 968–972, 2018, https://doi.org/10.1049/iet-rpg.2017.0698.

[46] Q. Su, F. Dong, and X. Shen, "Improved Adaptive Backstepping Sliding Mode Control of Static Var Compensator," *Energies*, vol. 11, no. 10, Oct. 2018, Art, no. 2750, https://doi.org/10.3390/en11102750.

[47] T. L. Nguyen, T. H. Vo, and N. D. Le, "Backstepping Control for Induction Motors with Input and Output Constrains," *Engineering, Technology & Applied Science Research*, vol. 10, no. 4, pp. 5998–6003, Aug. 2020, https://doi.org/10.48084/etasr.3680.

[48] N. Adhikary and C. Mahanta, "Integral backstepping sliding mode control for underactuated systems: Swing-up and stabilization of the Cart–Pendulum System," *ISA Transactions*, vol. 52, no. 6, pp. 870–880, Nov. 2013, https://doi.org/10.1016/j.isatra.2013.07.012.

[49] O. P. Bharti, R. K. Saket, and S. K. Nagar, "Controller Design For DFIG Driven By Variable Speed Wind Turbine Using Static Output Feedback Technique," *Engineering, Technology & Applied Science Research*, vol. 6, no. 4, pp. 1056–1061, Aug. 2016, https://doi.org/10.48084/etasr.697.

[50] H. Bassi and Y. A. Mobarak, "State-Space Modeling and Performance Analysis of Variable-Speed Wind Turbine Based on a Model Predictive Control Approach," *Engineering, Technology & Applied Science Research*, vol. 7, no. 2, pp. 1436–1443, Apr. 2017, https://doi.org/10.48084/etasr.1015.

[51] A. Maafa, H. Mellah, K. Ghedamsi, and D. Aouzellag, "Improvement of Sliding Mode Control Strategy Founded on Cascaded Doubly Fed Induction Generator Powered by a Matrix Converter," *Engineering, Technology & Applied Science Research*, vol. 12, no. 5, pp. 9217–9223, Oct. 2022, https://doi.org/10.48084/etasr.5166.

[52] "Design Loads for Horizontal Axis Wind Turbines," in *Wind Energy Handbook*, Hoboken, NJ, USA: John Wiley & Sons, Ltd, 2011, pp. 193–323.

[53] Labcontrol, "windturbineSim." [Online]. Available: https://github.com/labcontrol-data/windturbineSim.